JOURNAL OF BONE AND MINERAL RESEARCH
Volume 17, Number 8, 2002

Case Report

Synchrotron Radiation Microtomography Allows the Analysis of Three-Dimensional Microarchitecture and Degree of Mineralization of Human Iliac Crest Biopsy Specimens: Effects of Etidronate Treatment

S. NUZZO,[1,2] M.H. LAFAGE-PROUST,[3] E. MARTIN-BADOSA,[1,4] G. BOIVIN,[5] T. THOMAS,[3] C. ALEXANDRE,[3] and F. PEYRIN[1,2]

ABSTRACT

Quantitative microcomputed tomography using synchrotron radiation (SR μCT) was used to assess the effects of a sequential etidronate therapy on both three-dimensional (3D) microarchitecture and degree of mineralization of bone (DMB) in postmenopausal osteoporosis. Thirty-two iliac crest biopsy specimens were taken from 14 patients with osteoporosis (aged 64 ± 1.8 years) before (baseline) and after 1 year of etidronate treatment, and after 2 years of treatment for four of the patients. The samples were imaged at high spatial resolution (voxel size = 10 μm) using the microtomography system developed at the European Synchrotron Radiation Facility (ESRF), Grenoble, France. Three-dimensional microarchitecture parameters were calculated and compared with those obtained from conventional histomorphometry. In addition, the DMB was evaluated also in 3D. No significant statistical changes regarding bone mass and structural parameters were observed in histomorphometry or 3D analyses. The distribution of the DMB in cortical and trabecular bone showed a trend to a shift toward highest mineralization values after 1 year of etidronate treatment (3.88% and 1.24% in cortical and trabecular bone, respectively). This trend was more evident after 2 years. The study also showed that SR μCT is an accurate technique and the only one for quantifying both the mineralization and the microarchitecture of bone samples at the same time in 3D. (J Bone Miner Res 2002;17:1372–1382)

Key words: **bone architecture, degree of mineralization of bone, osteoporosis, quantitative microtomography, etidronate**

INTRODUCTION

It is well established that bisphosphonates (BPs) significantly reduce fracture incidence by decreasing bone turnover and increasing bone mineral density (BMD) assessed by DXA in patients with osteoporosis.[1–3] However, the mechanisms of BP action remain not fully understood. Indeed, although a significant increase in BMD of trabecular sites was observed in the alendronate-treated patients,[4] it was shown that no increase in bone mass (i.e., bone volume to total volume [BV/TV] from quantitative histomorphometry on iliac crest bone biopsy specimens) occurred in patients after a 3-year treatment with alendronate as compared with the placebo group. Significant increases in BMD

Dr. Peyrin received a grant from Procter and Gamble to pay for a student for 3 months. All other authors have no conflict of interest.

[1]ESRF, BP 220, Grenoble Cedex, France.
[2]CREATIS, Bat Blaise Pascal, INSA, Villeurbanne Cedex, France.
[3]INSERM E9901, St. Etienne Cedex 2, France.
[4]Laboratori d'"ptica, Departament de Física Aplicada i "ptica, Universitat de Barcelona, Barcelona, Spain.
[5]INSERM U403, Lyon Cedex 08, France.

also were observed in patients under other BPs,[1,5–7] including etidronate.[8,2] These data suggested that parameters other than true bone mass might explain changes in BMD or reduced fracture incidence under treatment. Several factors account for bone quality including three-dimensional (3D) microarchitecture, matrix composition, and degree of mineralization of bone (DMB). In fact, by reducing osteoclastic resorption, BPs might lessen the probability of trabeculae perforation in spongy bone,[9,10] and in cortical bone it was shown that they decrease bone porosity in ovariectomized primates.[11] In addition, Boivin et al.[12] recently showed that a 2- and 3-year treatment with alendronate was able to improve the mean DMB (MDMB) as compared with placebo, thus leading to an increase in BMD in the absence of actual changes in bone mass. As suggested by the authors, this phenomenon certainly is related to a more complete secondary mineralization of the basic structural units allowed by the reduced level of bone turnover.[13] In this latter work, the DMB was assessed on microradiography of bone slices obtained from ground-down biopsy specimens, which is the current reference technique. However, no data were available regarding concurrent changes in both 3D microarchitecture and DMB of human samples from patients under BP therapy.

Among the different techniques available, microcomputed tomography (μCT) is used increasingly to assess bone microarchitecture.[14] Synchrotron radiation μCT (SR μCT) may provide 3D images of bone samples with a spatial resolution as high as 1 μm.[15–17] Thus, specific image analysis procedure may be applied to these 3D images to get morphological and topological quantitative parameters.[18,19] SR μCT was used to study the relationships between 3D architecture and the elastic properties of trabecular bone in humans[20] and rats.[21] So far, the possibility of obtaining quantitative information regarding the mineral content of different areas of bone using μCT has not been exploited. The technique relies on the physical properties of SR, which allows reconstructing quantitative maps of the 3D distribution of linear absorption coefficient within volumetric samples. Because absorption depends on the amount of mineral in bone, a suitable calibration is able to relate the reconstructed gray levels in SR μCT images to the local DMB.

In this context, our aim was to use SR μCT to analyze two elements of bone quality, that is, 3D microarchitecture and DMB in patients with osteoporosis before and after a 1-year etidronate treatment.

MATERIALS AND METHODS

Patients and treatment

Fourteen postmenopausal patients with osteoporosis (aged 64 ± 1.8 years), with a mean of 2.1 ± 1.3 vertebral crush fractures, underwent a bone iliac crest biopsy after double tetracycline labeling at baseline and after 1 year of sequential treatment including etidronate (400 mg/day for 14 days; Procter and Gamble, Cincinnati, OH, USA) followed by a 1-g/day supplement of elemental calcium (Calcium Sandoz Forte; Sandoz Pharmaceuticals, Inc., East Hanover, NJ, USA) for 2.5 months. This 13-week cycle was repeated four times. Among the 14 patients, 4 patients were followed up 1 more year under a similar therapy and a third biopsy was performed on the iliac crest that was operated on at baseline. These 14 patients were a subgroup of a population of 32 subjects with osteoporosis, submitted to etidronate, whom histomorphometric results at baseline and after 1 year of treatment were reported previously.[22] After biopsy, bone samples were embedded in resin and processed for histomorphometry (see the following section). The 14 biopsy specimens, which were selected from the original group for this study, were the ones with a substantial amount of bone available (at least more than one-half of the bone sample still remaining in the plastic block). These blocks (~7 × 7 × 10 mm) were used for SR μCT measurements.

Bone histomorphometry

Iliac crest bone biopsy specimens were embedded in a resin made of purified glycol and methylmethacrylate at 4°C. Nonserial sagittal 7-μm-thick sections were carried out on a Reichert microtome (Cambridge Instruments GmbH, Nublock, Germany). Sections were stained with modified Goldner for subsequent measurements of conventional bone histomorphometry.[23] Measurements of BV (BV/TV, percent of cancellous bone area) and calculation of structural indices (trabecular thickness [Tb.Th] and trabecular number [Tb.N]) were carried out on an automatic image analyzer (Biocom, Lyon, France). Five sections per individual were measured. The bone formation rate (BFR/bone surface [BS]) was measured on five unstained sections under UV light. It was calculated as the product of the mineral apposition rate (MAR) and of the mineralizing surface (MS/BS, percentage of double-labeled bone perimeter ± one-half percentage of single-labeled bone perimeter).

All biopsy specimens were observed thoroughly to detect any mineralization impairment or alteration in bone quality, that is, woven bone or microcallus.

Microtomographic image acquisition

Measurements were carried out on the high-resolution diffraction and topography beam-line ID19. The detailed description of the experimental device for tomographic scans was reported elsewhere.[24] The setup is based on a 3D parallel tomographic acquisition. A monochromatic X-ray beam was selected using a double crystal silicon monochromator, operating in the symmetrical Bragg reflection geometry. The 3D distribution of the internal structure of the sample was reconstructed from a set of 2D projections under different angles of view. For each bone sample, 900 radiographic images were acquired over an angular range of 180°, (angular step, 0.2°). The transmitted X-ray beam after the sample was recorded using a scintillator coupled to a 2D CCD-based camera, the FRELON camera developed by the European SR facility (ESRF) Detector Group.[25] It includes 1024 * 1024 elements with a pixel size of 19 μm and a dynamic range of 14 bits. For these experiments, the X-ray energy was set to 20 KeV and the optical system was fixed

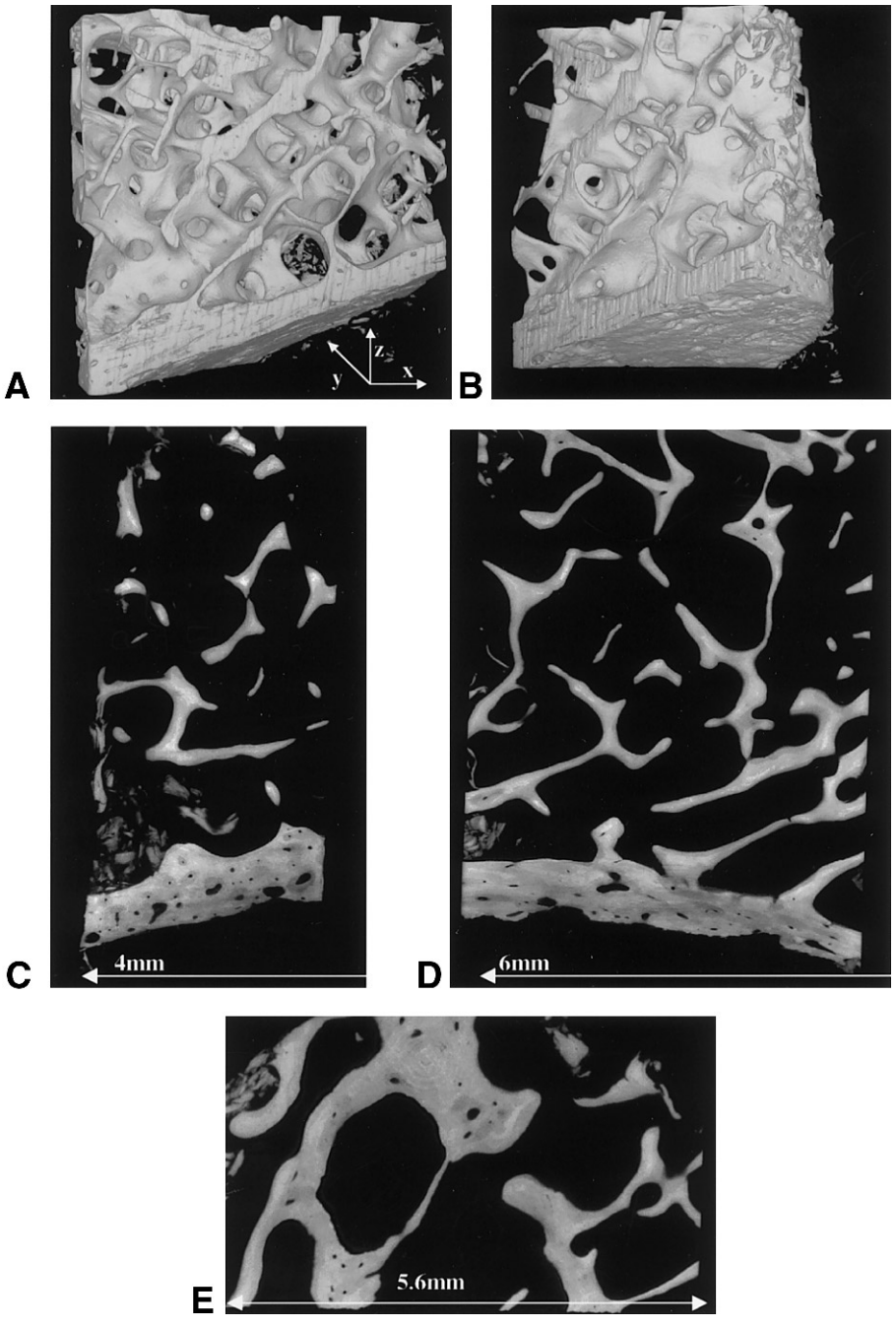

FIG. 1. Three-dimensional SR μCT reconstructed image from an iliac crest biopsy. (A–B) Three-dimensional displays at two different angles of view. (C–E) Two-dimensional slices through the 3D image. (C) Slice x = 142; (D) slice y = 255; (E) slice z = 26.

to get a pixel size of 10.13 μm. This pixel size yields a 10 mm $\times$ 10 mm field of view for each radiograph. The exposure time for one image was about 0.7 s so that the total scan of each sample lasted for less than 15 minutes. During the experiment, the operation mode of the machine was multibunch mode with a current of $\sim$200 mA. Dark current and reference images without the sample were taken regularly to perform a flat field correction. The lacks of spatial homogeneity of the beam and of the individual pixel detector responses for the most part were eliminated. The corrected projection images then were processed with an exact tomographic reconstruction algorithm based on 3D filtered back-projection algorithm. Volumes of $\sim 600 * 500 * 900$ cubic voxels (size, 10.13 μm) were reconstructed. As an illustration, Fig. 1 shows, respectively, a 3D display of bone surfaces and three orthogonal slices through a reconstructed bone biopsy volume. Because of the quality of images in terms of spatial resolution and signal-to-noise ratio, bone structure could be segmented easily from background by simple thresholding. From a qualitative point of view, it is noteworthy that differences in gray levels could be observed on the slices both in cortical and in trabecular regions. This property allowed a clear visualization of the typical shapes of bone packets.

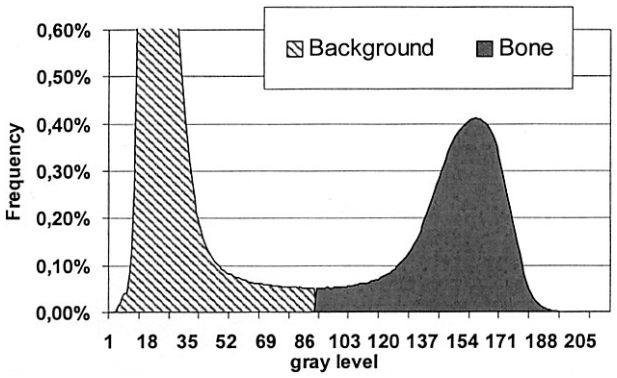

FIG. 2. Typical histogram of the gray levels of a 3D SR μCT image.

Analysis of 3D architecture

3D SR μCT images ideally are suited to perform accurate architectural analysis. For each patient, 3D architectural parameters were computed in selected regions of interest (ROIs) of trabecular bone. These ROIs were chosen within the internal part of trabecular bone to avoid cracks and fragments due to biopsy taking and histomorphometry cutting off. Because of these constraints, the size of each ROI was not the same for all biopsy samples. The number of voxels in the *x*, *y*, and *z* directions ranged from 300 to 500, 200 to 300, and 300 to 600, respectively. Figure 2 shows a typical histogram in a trabecular ROI. Because of the good contrast and the high spatial resolution of images, bimodal histograms were obtained. The first peak (low gray levels) corresponds to resin and background absorption, and the second one corresponds to bone absorption. Thus, bone structure was binarized by simple thresholding, with the same threshold for each sample of the series.

Different methods are available for architecture analysis.[26] The 3D mean intercept length (MIL) method[18] was used first and delivered morphometry and anisotropy parameters. The 3D image was scanned by a 3D test grid for random orientations and the number of secants of parallel test lines with bone were evaluated. The following parameters were extracted assuming a parallel plate model: BV/TV (%), BS/BV (mm^{-1}), Tb.Th (μm), Tb.N (mm^{-1}), trabecular separation (Tb.Sp; μm). This analysis was applied to cubic subvolumes in trabecular ROIs.

Because 3D images provide complete information on the BV, it is not necessary to make model assumptions, and we also used direct 3D parameters. The Tb.Th* was computed according to the definition proposed by Hildebrand.[19] The algorithm does not require any special constraints regarding both the size and the geometry of BVs. The same method was applied to the background instead of bone structure to evaluate a direct Tb.Sp*. The direct BS/BV* was calculated from a triangular mesh of the BSs. A direct Tb.N* also was calculated as BV/TV/Tb.Th*. Moreover, the connectivity of trabecular bone samples was estimated from the computation of the Euler number as previously described.[27] The connectivity was normalized to the TV and expressed (in mm^{-3}). The architecture parameters also were computed on the first slice of each volume reconstructed for comparison to histomorphometry.

The correlation coefficients between the 3D and 2D homologous parameters were calculated to compare the different techniques used (histology, MIL, and direct method) for the evaluation of 2D and 3D architectural parameters.

Analysis of the DMB

Calibration technique: At the difference to the CT number of clinical X-ray scanners, the gray levels in the 3D reconstructed SR μCT images correspond to the linear attenuation coefficient for a given energy. Because absorption depends on the mineral composition of bone, a suitable calibration method allows estimating of the 3D distribution of mineral content within a bone sample. To calibrate the gray level (i.e., the absorption attenuation coefficient) into the mineral part of bone tissue, we used phantoms of homogeneous water solutions with different dipotassium hydrogen phosphate (K_2HPO_4) concentrations. The samples were imaged in the same experimental conditions used for the bone samples (energy, 20 keV; pixel size, 10.13 μm). The method was compared with microradiography based on an aluminum step-wedge calibration.[28,29] For this purpose, the same 100-μm-thick section of bone was radiographed both at the ESRF at 8 keV, and at the U403 INSERM Unit (Lyon, France) using a nickel-filtered copper K_{74} radiation with a wavelength of 1.54 Å (E ~ 8 keV). Figure 3A illustrates the same cortical bone slice imaged with the two techniques, displaying similar contrasts. The gray levels were converted into their corresponding degree of mineralization values by using both calibration methods. The histograms representing the number of pixels as a function of mineral content per cubic centimeter of bone, obtained from the two techniques, were not directly at the same scale because the steps in DMB were different. To compare the results, we estimated the probability density function (pdf), respectively, from both histograms. Figure 3B shows the pdf's of the DMB using the two methods in both ROIs displayed in Fig. 3A. It may be seen that the two curves are well overlaid and exhibit the same range of variation of the DMB of 0.6–1.3 g/cm^3 in cortical bone. The same result was found in both trabecular and cortical regions, as well as in total bone (cortical + trabecular). The MDMB for the different bone regions are reported in Table 1. The relative errors were calculated as the absolute differences in DMB mean value between SR μCT and microradiography. The mean difference is ~4.21%, indicating a good agreement between the two techniques.

3D analysis of the DMB: The DMB was quantified separately in the trabecular ROIs already used for architectural analysis and in additional cortical ROIs carefully selected from the 3D biopsy volumes. The number of voxels in the cortical ROIs along the *x*, *y*, and *z* directions ranged from 300 to 500, 200 to 300, and 60 to 120, respectively. The distribution of the gray levels within the different ROIs was obtained from the histogram of the bone images normalized by the TV. The gray levels corresponding to bone absorption were converted into concentrations of mineral content (in g/cm^3 of bone) according to the calibration method. The

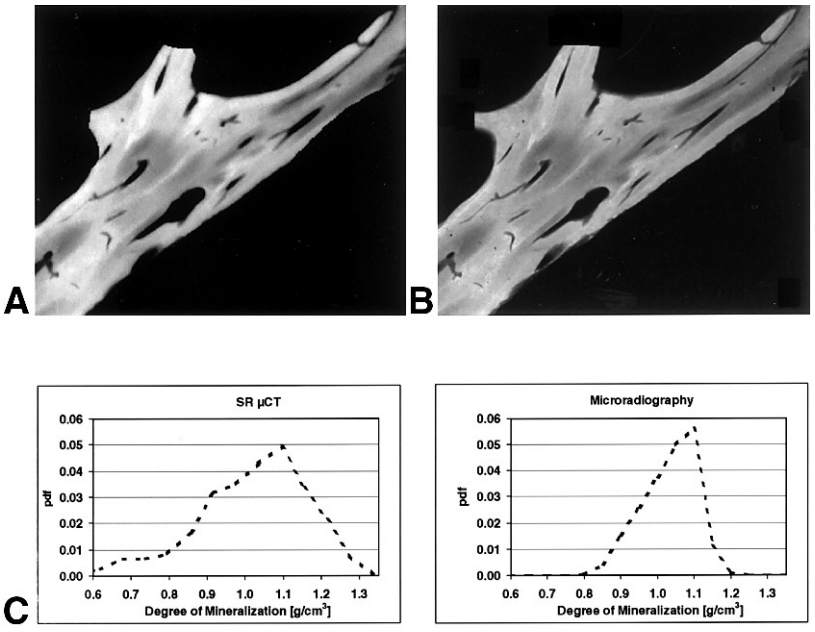

FIG. 3. Images of the same 100-μm-thick slice of cortical bone (A) SR image, (B) microradiograph, and (C) corresponding pdf estimated by the two calibration methods.

TABLE 1. MDMB AND BETWEEN BRACKETS THE SD, CALCULATED FOR THE TRABECULAR AND CORTICAL REGION OF THE SAME BONE FRAGMENT MEASURED BY USING SR μCT AND MICRORADIOGRAPHY

MDMB	*SR μCT*	*μRadiography*	*ΔMDMB*
Trabecular	1.00 (0.05)	1.12 (0.07)	4.14%
Cortical	1.08 (0.05)	1.05 (0.06)	4.11%
Total	1.18 (0.06)	1.13 (0.08)	4.39%

The relative error ΔMDMB comparing results from the two techniques also are indicated for each bone region.

histograms were averaged for each group. The changes (ΔDMB) after treatment were calculated as the relative percentage of the baseline value for each patient. Afterward, the mean ΔDMB value was determined for each group.

Statistical analysis

Descriptive statistics including, the mean, SD, minimum, and maximum values were evaluated for each group of patients for both microarchitecture parameters and DMB. The three groups of patients, before treatment, after 1 year and 2 years of etidronate (ETD) are, respectively, denoted baseline, ETD1, and ETD2. To evaluate the effects of etidronate, the values of all parameters (architectural, DMB, and histodynamic parameters) obtained at baseline were compared with those after a 1-year treatment ($n = 14$) using a T-Wilcoxon test. The Spearman correlation coefficient was calculated to investigate potential correlations between the different techniques (i.e., conventional histomorphometry, SR μCT direct, and MIL methods). Finally, a linear regression analysis was carried out between BFR/BS and the DMB.

RESULTS

Conventional histomorphometric results

Data are summarized in Table 2. Bone mass and structural parameters did not show any significant change after 1-year treatment with etidronate. In contrast, histodynamic measurements showed a significant decrease in BFR/BS after 1-year treatment, confirming the expected etidronate-induced reduction in bone turnover. This decrease in BFR occurred through both a decrease in MAR (0.70 ± 0.07 μm/day at baseline vs. 0.49 ± 0.10 μm/day; $p < 0.01$) and in MS/BS ($8.1 \pm 4.9\%$ at baseline vs. $3.5 \pm 2.6\%$; $p < 0.001$). Thorough observation of the sections did not reveal either mineralization impairment or signs of bone quality damage such as woven bone, microcracks, or microcallus. Moreover, measurement of mineralization lag time, osteoid thickness, and osteoid volume ruled out focal and atypical osteomalacia in these samples (data not shown).

3D architecture results

3D parameters calculated using MIL and direct methods are reported in Tables 3 and 4, respectively. The statistical analysis showed no significant changes in bone mass and structural parameters after 1-year treatment as compared with baseline. The correlation coefficients of the different parameters are summarized in Table 5. Bone mass and structural parameters, measured with conventional histomorphometry, fairly correlated with those measured with SR μCT (BV/TV, $r' = 0.79$ and $p < 0.0001$; Tb.N, $r' = 0.78$ and $p < 0.0001$; Tb.Sp, $r' = 0.82$ and $p < 0.0001$) except for Tb.Th ($r' = 0.5$, not significant). High positive correlations were observed when comparing the 3D parameters extracted by the direct method and the MIL approach. The weakest correlation was found for Tb.Th measurements.

TABLE 2. BONE MASS AND ARCHITECTURAL AND BONE FORMATION HISTOMORPHOMETRIC PARAMETERS IN PATIENTS AT BASELINE AND AFTER 1 YEAR (ETD1) OR 2 YEARS (ETD2)

	Baseline	*ETD1*	*Baseline*	*ETD1*	*ETD2*
	n = *14 patients*		n = *4 patients*		
BV/TV (%)	15.2 ± 5.5	14.8 ± 4.5	16.2 ± 4.1	17.8 ± 5.8	15.9 ± 4.5
Tb.Th (μm)	126.5 ± 28.2	116.6 ± 39.1	130.6 ± 14.9	114.0 ± 41.8	112.6 ± 29.4
Tb.N (mm^{-1})	1.20 ± 0.33	1.3 ± 0.31	1.28 ± 0.20	1.41 ± 0.26	1.38 ± 0.12
Tb.Sp (μm)	774.1 ± 296.8	691.9 ± 194.7	668.4 ± 158.2	593.3 ± 113.7	575.1 ± 54.2
BFR/BS ($\mu m^3/\mu m^2$ per day)	0.045 ± 0.020	0.027 ± 0.018*	0.070 ± 0.015	0.019 ± 0.013	0.014 ± 0.015

* Versus baseline, $p < 0.05$.

TABLE 3. BONE MASS AND ARCHITECTURAL AND 3D PARAMETERS OBTAINED BY USING THE MEAN MIL METHOD, IN PATIENTS AT BASELINE AND AFTER 1 YEAR (ETD1) OR 2 YEARS (ETD2)

	Baseline	*ETD 1 year*	*Baseline*	*ETD1*	*ETD2*
3D MIL	n = *14 patients*		n = *4 patients*		
BV/TV (%)	14.5 ± 5.9	13.9 ± 4.6	18.5 ± 1.6	17.1 ± 4.1	21.2 ± 4.7
(min–max)	(5.6–23.9)	(6.2–22.0)	(16.7–20.6)	(10.9–22.0)	(15.2–28.1)
BS/BV (mm^{-1})	23.5 ± 5.9	24.5 ± 6.3	19.5 ± 1.44	23.4 ± 8.4	20.8 ± 3.2
(min–max)	(14.6–32.4)	(15.9–37.6)	(18.4–21.9)	(15.9–37.6)	(16.1–25.2)
Tb.Th (μm)	91 ± 23	85 ± 22	92 ± 18	93 ± 23	99 ± 16
(min–max)	(61–137)	(53–121)	(63–108)	(53–109)	(79–125)
Tb.N (mm^{-1})	1.5 ± 0.4	1.6 ± 0.4	1.8 ± 0.3	1.8 ± 0.1	2.1 ± 0.2
(min–max)	(0.9–2.3)	(0.4–1.1)	(1.5–2.3)	(1.7–2.0)	(1.9–2.4)
Tb.Sp (μm)	611 ± 200	582 ± 188	462 ± 71	452 ± 15	374 ± 52
(min–max)	(351–1039)	(392–1062)	(351–538)	(436–477)	(317–442)

3D results on DMB

The gray level distribution allowing the study of bone mineral content was evaluated from the bone peak of the histogram, first normalized to the BV of each biopsy specimen. The concentration in mineral substance after calibration was found in the range of 0.6–1.3 g/cm^3 in both cortical and trabecular bone. The averaged distributions of mineral content for each group (baseline, ETD1, and ETD2) are illustrated in Fig. 4. It is remarkable to note that changes in the DMB under treatment differed between bone envelopes. In cortical bone, values shifted toward higher degrees of mineralization along with a decrease of the lowest degrees. In trabecular bone, only the lowest values decreased. MDMB are reported in Table 6. The differences between the individual DMB values for the two groups were found in the CI of 10%, for both trabecular and cortical envelopes. After 2 years, the MDMB increased by ~12% and 8% in cortical and trabecular bone, respectively. The peak corresponding to the bone absorption region clearly showed a shift toward the right side or highest mineralized values. Interestingly, a significant negative relationship between BFR/BS and the DMB values was found in all etidronate-treated patients ($n = 18$) while no such relationship was observed at baseline (Fig. 5).

DISCUSSION

A few years ago, the World Health Organization added to the definition of osteoporosis, characterized as a systemic skeletal disease inducing a decrease in bone mass leading to fracture, the notion of a deterioration of bone architecture,[30] thus emphasizing the role of trabecular connectivity in bone resistance to fracture. Indeed, some but not all biomechanical properties correlate with bone density.[31,32] Ex vivo tests showed that 70–90% of the variance of bone elastic modulus and strength is explained by linear and power functions of bone density depending on the bone site.[33,34] However, clinical studies showed a substantial overlap between BMD values of individuals with bone fractures and those without.[35] Trabecular 3D organization (connectivity and orientation of the trabeculae) as well as bone tissue intrinsic quality might explain the remaining 20–30% of the bone mechanical properties variance. Indeed, studies evaluating concurrently bone mechanical properties, bone mass, and microarchitecture showed that bone strength and elastic modulus were better predicted when including microarchitecture parameters than when using bone mass alone.[36–38] Various techniques were developed to visualize and measure microarchitecture including histomorphometry, serial histological sections followed

Table 4. Direct 3D Architectural Parameters in Patients at Baseline and After 1 Year (ETD1) or 2 Years (ETD2)

	Baseline	*ETD 1 year*	*Baseline*	*EDT1*	*ETD2*
3D Direct	n = *14 patients*		n = *4 patients*		
BV/TV* (%)	15.2 ± 6.4	14.5 ± 5.1	19.4 ± 2.0	18.0 ± 5.6	22.2 ± 6.0
(min–max)	(5.8–24.8)	(5.6–24.0)	(17.6–21.8)	(11.2–3.5)	(16.0–29.2)
BS/BV* (mm^{-1})	20.3 ± 4.8	24.5 ± 6.5	17.5 ± 1.7	20.2 ± 7.6	18.1 ± 2.7
(min–max)	(13.2–27.2)	(15.9–37.6)	(18.4–21.9)	(14.9–30.8)	(14.8–20.7)
Tb.Th* (μm)	180 ± 40	172 ± 37	196 ± 15	178 ± 54	187 ± 27
(min–max)	(121–246)	(103–227)	(177–212)	(102–227)	(164–223)
Tb.N* (mm^{-1})	1.5 ± 0.4	1.6 ± 0.4	1.8 ± 0.3	1.9 ± 0.2	2.1 ± 0.2
(min–max)	(0.9–2.3)	(0.9–2.1)	(1.5–2.3)	(1.7–2.0)	(1.9–2.4)
Tb.Sp* (μm)	701 ± 62	682 ± 64	684 ± 83	660 ± 40	573 ± 56
(min—max)	(516–814)	(572–789)	(561–747)	(603–698)	(515–650)
Connectivity (mm^{-3})	4.5 ± 2.2	5.4 ± 3.6	4.9 ± 2.0	5.0 ± 1.8	10.2 ± 6.4
(min–max)	(1.3–8.7)	(1.4–15.6)	(3.4–7.8)	(2.8–6.7)	(3.9–18.0)

Table 5. Spearman Correlation Coefficients Between Microarchitectural Parameters Computed From Histomorphometry (2D), 3D MIL, and 3D Direct Methods

	BV/TV	*BS/BV*	*Tb.Th*	*Tb.N*	*Tb.Sp*
3D MIL/3D Direct	0.98*	0.98*	0.96*	0.97*	0.87*
2D/3D MIL	0.79*	—	0.50	0.78*	0.82*
2D/3D MIL first slice	0.78*	—	0.84*	0.82*	0.84*

* The statistical significance ($p < 0.0001$) is indicated by *. "3D MIL first slice" corresponds to the parameters extracted from the first slice of each volume reconstructed.

by 3D reconstruction,[39] quantitative μCT,[40] or magnetic resonance imaging.[41,42] According to Parfitt et al.,[43,44] the mathematic parallel plate model allows extrapolation of 3D parameters such as Tb.Th or Tb.N from bidimensional measurements of trabecular bone perimeter and trabecular bone area. This latter technique was used extensively in humans and animals for studying osteoporosis pathophysiology or treatments. Compared with reconstruction based on serial histological sections, which is time consuming and rarely performed,[45] μCT, pioneered by Feldkamp et al.,[46] appears to be a suitable method for imaging and quantifying trabecular bone microstructure in 3D[14] in animals and in humans.[47]

The use of SR μCT as compared with standard μCT offers the opportunity of an accurate investigation of local bone mineral content in addition to microarchitectural analysis. Present results report the first simultaneous analysis of both 3D microarchitecture and DMB in biopsy specimens previously processed for conventional histomorphometry, with no further destruction of the sample.

We found fair correlations between histomorphometric (2D) and 3D homologous parameters, which were comparable with previously reported results.[48] Interestingly, the histomorphometric Tb.Th exhibited the weakest correlation with the 3D MIL technique ($r' = 0.5$). This correlation was much higher when the 3D calculation was limited to the first slice closest to that of histology ($r' = 0.84$). These results permit validation of SR μCT as compared with histology, which is used widely and still considered as the standard technique for the study of bone microarchitecture. However, the values obtained in 2D measurements can significantly differ depending on the position and on the direction of the slice. Thus, 3D analysis allows overcoming the strong variability of 2D measurements because of the larger number of slices used in the computation.

The methods used for the calculation of morphological parameters yielded significant differences for some parameters. Although the BV/TV and BS/BV parameters were very close for 3D direct and indirect methods, the other parameters presented substantial absolute variations. For instance, the direct Tb.Th* generally was higher than the Tb.Th derived from the parallel plate model. The same behavior was already observed in a previous work reporting microstructural data obtained from standard μCT on different bone sites.[49] The orders of magnitude between the values reported on iliac crest biopsies in the later work were the same as in our findings. The differences between direct and indirect methods suggest that the assumption of a parallel plate model is not completely appropriate. However, most correlations between 3D parameters were quite high. A smaller correlation may be observed between Tb.Sp from the parallel plate model and its 3D direct homologous, and the values are quite different.

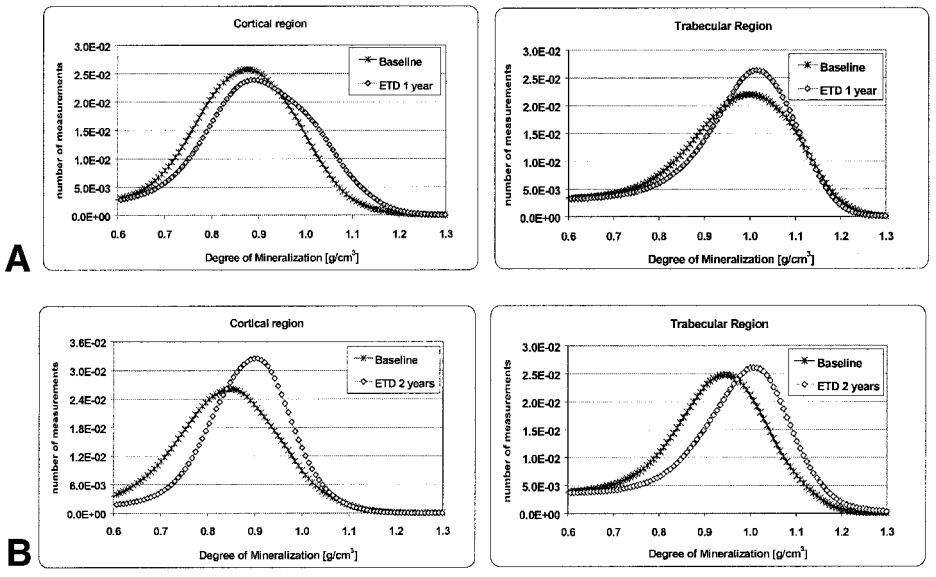

FIG. 4. Distributions of the DMB (in mineral content per cubic centimeter of bone) in patients at baseline and after etidronate treatment at (A) 1 year (n = 14 patients, EDT1) and (B) 2 years (n = 4 patients, ETD2).

TABLE 6. EFFECTS OF ETIDRONATE TREATMENT ON BONE MINERALIZATION

Mean DMB (SEM; g/cm³)	*Baseline*	*ETD1*	*Baseline*	*ETD1*	*ETD2*
	n = *14 patients*		n = *4 patients*		
Cortical bone	0.871 (0.011)	0.901 (0.012)	0.846 (0.010)	0.902 (0.012)	0.948 (0.013)
Mean ΔDMB (%)		+3.88		+4.09	+12.07
Trabecular bone	0.940 (0.014)	0.951 (0.014)	0.880 (0.013)	0.910 (0.013)	0.952 (0.015)
Mean ΔDMB (%)		+1.24		+1.39	+8.26

Mean values of DMB and the SEM calculated for each averaged histogram over the different groups. The second line indicates the mean ΔDMB percentage of the baseline, averaged over the different groups.

In this study, after 1 year of etidronate treatment, neither bone volume nor microarchitecture parameters, including connectivity, changed while the dynamic indices of bone remodeling such as BFR/BS had significantly decreased. This lack of effect on bone mass was not caused by the weak potency of etidronate because similar results were reported with other more potent BPs such as pamidronate[50] or alendronate.[4] Thus, etidronate did not improve the connectivity parameters. However, in the absence of a control group, we cannot rule out the possibility that etidronate prevented further microarchitectural deterioration.

Using a gray-level scale, DMB currently is assessed by microradiography, which is the gold standard for this evaluation.[12] However, before microradiography assessment, it is necessary to obtain regular, thin (100 μm thick), and evenly polished bone slices, which is a very time-consuming procedure. Conversely, there is no need for special sample preparation to perform 3D SR μCT images. In addition, 3D measurements give information from a stack of virtual slices at the same time; thus, results are statistically more representative and robust than when obtained from a single slice. Currently, standard μCT is used to assess 3D bone microarchitecture but has never been used yet for the quantification of the DMB. The present method, based on a monochromatic X-ray beam, provided by SR makes this quantification possible directly in 3D because of the lack of beam hardening.

In our study, the etidronate-induced changes did not reach but were close to the level of statistical significance ($p < 0.05$) after the first year of treatment. The MDBM tended to increase in both envelopes. After 2 years of treatment the shift of the curves toward the high values became more apparent, although the number of patients available was very limited. These changes in mineralization under BPs were thought related to an increase in the duration of the secondary mineralization phase because of the reduction in bone remodeling. Data showing a significant negative relationship between BFR/BS and MDBM only in etidronate-treated patients support this hypothesis. Moreover, it was assumed that this increase in MDBM could account for the improved bone strength. This assumption was supported by the fact that the mineralization of bone matrix concurs with its mechanical properties[51] and by the decrease of fracture rate reported in BP-treated patients.[4,12] Indeed, it was shown, in alendronate-treated minipigs that there was a negative relationship between the level of bone remodeling

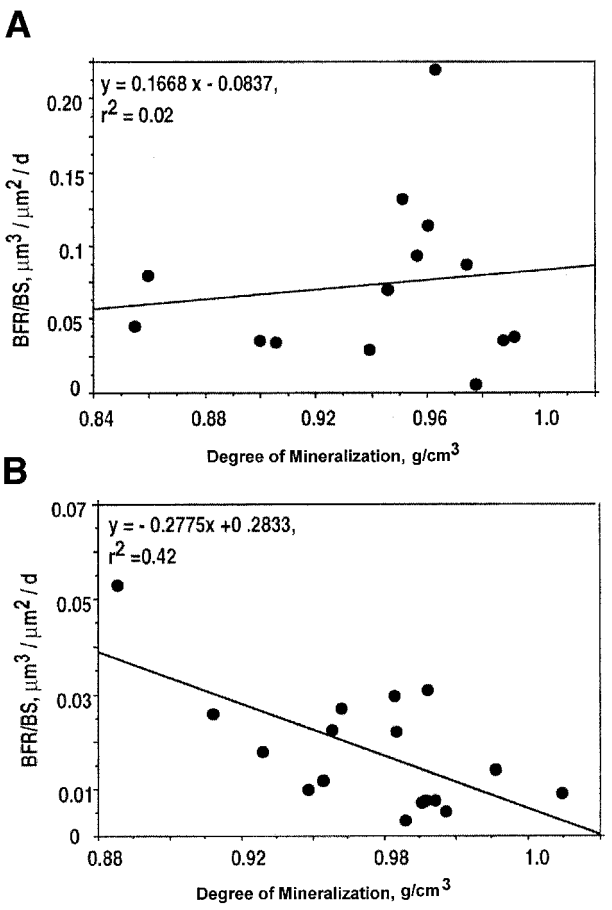

FIG. 5. Linear regression relationship between BFR/BS and DMB (A) in patients at baseline ($n = 14$) and (B) in all patients treated by etidronate ($n = 18$; $p < 0.01$).

and both the cortical and the trabecular bone resistance to fracture.[52] However, by reducing bone remodeling levels, BPs might increase collagen cross-links as well and thus improve bone matrix mechanical properties as it was reported previously.[53] In addition, the importance of a correct level of cross-linking for mineralization also was reported,[54,55] emphasizing the major role of the mineral/matrix interface.

In conclusion, our results clearly showed that SR μCT is a useful and innovative tool for bone quality analysis. It allows information on both mineralization and trabecular microarchitecture of the same bone samples. Moreover, we found that etidronate, a first generation BP, was able to induce changes in bone mineralization as early as the first year of treatment, whereas no change in bone microarchitecture parameters was observed. After 2 years of treatment, the changes in mineralization are similar to those reported with alendronate,[12] suggesting that these effects may be shared by drugs reducing bone remodeling. Whether this increase in bone mineralization accounts for the increase in bone strength and related decrease in fracture rate remains to be determined.

ACKNOWLEDGMENTS

The authors thank the ESRF for financial support, J. Baruchel for his valuable input into this project, and P. Cloetens for his useful help during microtomography experiments. We gratefully acknowledge R. Chagnon and D. Rolhion for mechanical support, D. Fernández-Carreiras, Beam Line Instrumentation Software Support (BLISS), for computing assistance, and the ESRF Detector Group for assistance with the detector.

REFERENCES

1. Black DM, Cummings SR, Karpf DB, Cauley JA, Thompson DE, Nevitt MC, Bauer DC, Genant HK, Haskell WL, Marcus R, Ott SM, Torner JC, Quandt SA, Reiss TF, Ensrud KE 1996 Randomised trial of effect of alendronate on risk of fracture in women with existing vertebral fractures. Fracture Intervention Trial Research Group. Lancet **7:**1535–1541.
2. Watts NB, Harris ST, Genant HK, Wasnich RD, Miller PD, Jackson RD, Licata AA, Ross P, Woodson GC, Yanover MJ, Mysim J, Kohse L, Rao MB, Steiger P, Chesnut CH 1990 Intermittent cyclical etidronate treatment of postmenopausal osteoporosis. N Engl J Med **12:**73–79.
3. Harris ST, Watts NB, Genant HK, McKeever CD, Hangartner T, Keller M, Chesnut CH III, Brown J, Eriksen EF, Hoseyni MS, Axelrod DW, Miller PD 1999 Effects of risedronate treatment on vertebral and non vertebral fractures in women with postmenopausal osteoporosis: A randomized controlled trial. Vertebral Efficacy with Risedronate Therapy (VERT) Study Group. JAMA **13:**1344–1352.
4. Chavassieux PM, Arlot ME, Reda C, Wei L, Yates AJ, Meunier PJ 1997 Histomorphometric assessment of the long-term effects of alendronate on bone quality and remodeling in patients with osteoporosis. J Clin Invest **15:**1475–1480.
5. Schneider PF, Fischer M, Allolio B, Felsenberg D, Schroder U, Semler J, Ittner JR 1999 Alendronate increases bone density and bone strength at the distal radius in postmenopausal women. J Bone Miner Res **14:**1387–1393.
6. Hanley DA, Ioannidis G, Adachi JD 2000 Etidronate therapy in the treatment and prevention of osteoporosis. J Clin Densitom **3:**79–95.
7. Crilly RG, Sebaldt RJ, Hodsman AB, Adachi JD, Brown JP, Goldsmith CH, Hanley DA, Olszynski WO, Ste-Marie LG, Stephenson GF 2000 Predicting subsequent bone density response to intermittent cyclical therapy with etidronate from initial density response in patients with osteoporosis. Osteoporos Int **11:**607–614.
8. Storm T, Thamsborg G, Steiniche T, Genant HK, Soresen OH 1990 Effect of intermittent cyclical etidronate therapy on the bone mass and fracture rate in women with postmenopausal osteoporosis. N Engl J Med **322:**1265–1271.
9. Barou O, Lafage-Proust MH, Martel C, Thomas T, Tirode F, Laroche N, Barbier A, Alexandre C, Vico L 1999 Bisphosphonate effects in rat unloaded hindlimb bone loss model: Three-dimensional microcomputed tomographic, histomorphometric, and densitometric analyses. J Pharmacol Exp Ther **291:**321–328.
10. Parfitt AM 1992 Implications of architecture for the pathogenesis and prevention of vertebral fracture. Bone **13**(Suppl 2)**:** 41–47.
11. Balena R, Lafage MH, Markatos A, Seedor JG, Rodan GA 1992 The effect of two years alendronate treatment on cortical bone remodeling. J Bone Miner Res **7:**S329 (abstract).
12. Boivin GY, Chavassieux PM, Santora AC, Yates J, Meunier PJ 2000 Alendronate increases bone strength by increasing the

mean degree of mineralization of bone tissue in osteoporotic women. Bone **27:**687–694.
13. Meunier PJ, Boivin GY 1997 Bone mineral density reflects bone mass but also the degree of mineralization of bone: Therapeutic implications. Bone **21:**373–377.
14. Ruegsegger P, Koller B, Müller R 1996 A microtomographic system for the nondestructive evaluation of bone architecture. Calcif Tissue Int **58:**24–29.
15. Engelke K, Graeff W, Meiss L, Hahn M, Delling G 1993 High spatial resolution imaging of bone mineral using computed microtomography Comparison with microradiography and undecalcified histologic sections. Invest Radiol **28:**341–349.
16. Peyrin F, Salomé M, Nuzzo S, Cloetens P, Laval-Jeantet AM, Baruchel J 2000 Perspectives in Three-dimensional analysis of bone samples using synchrotron radiation μCT. Cell Mol Biol **46:**1089–1102.
17. Bonse U, Busch F, Gunnewig O, Beckmann F, Pahl R, Delling G, Hahn M, Graeff W 1994 3D computed X-ray tomography of human cancellous bone at 8 microns spatial and $10^{(-4)}$ energy resolution. Bone Miner **25:**25–38.
18. Hipp JA, Simmons CA 1997 Method-based differences in the automated analysis of the three-dimensional morphology of trabecular bone. J Bone Miner Res **12:**942–947.
19. Hildebrand T, Rüegsegger P 1997 A new method for the model independent assessment of thickness in three-dimensional images. J Microsc **187:**67–75.
20. Kinney JH, Ladd AJ 1998 The relationship between three-dimensional connectivity and the elastic properties of trabecular bone. J Bone Miner Res **13:**839–845.
21. Kinney JH, Haupt DL, Balooch M, Ladd AJ, Ryaby JT, Lane NE 2000 Three-dimensional morphometry of the L6 vertebra in the ovariectomized rat model of osteoporosis: Biomechanical implications. J Bone Miner Res **15:**1981–1991.
22. Thomas T, Barou O, Vico L, Alexandre C, Lafage-Proust MH 1999 Recurrence of vertebral fracture with cyclical etidronate therapy in osteoporosis: Histomorphometry and X-ray microanalysis evaluation. J Bone Miner Res **14:**198–205.
23. Parfitt AM, Glorieux F, Kannis H, Malluche A, Meunier PJ, Ott SM, Recker RR 1987 Bone histomorphometry nomenclature symbols and units Report of the ASBMR Histomorphometry Nomenclature. J Bone Miner Res **2:**595–610.
24. Salomé M, Peyrin F, Cloetens P, Odet C, Laval-Jeantet AM, Baruchel J, Spanne P 1999 A synchrotron radiation microtomography system for the analysis of trabecular bone samples. Med Phys **26:**2194–2204.
25. Labiche JC, Segura-Purchades J, Van Brussel D, Moy JP 1996 FRELON camera: Fast read low noise. ESRF NewsLetter **25:**41–43.
26. Odgaard A 1997 Three-dimensional methods for quantification of cancellous bone architecture. Bone **20:**315–328.
27. Odgaard A, Gundersen HJG 1993 Quantification of connectivity in cancellous bone with special emphasis on 3D reconstructions. Bone **14:**173–182.
28. Sissons HA, Jowsey J, Stewart L 1960 Quantitative microradiography of bone tissue. In: Engström A, Cosslett V, Pattee H (eds.) X-Ray Microscopy and X-Ray Microanalysis. Elsevier, Amsterdam, The Netherlands, pp. 199–205.
29. Boivin G, Baud CA 1984 Microradiographic methods for calcified tissue. In: Dickson GR (ed.) Methods of Calcified Tissue Preparation, pp. 391–412.
30. Consensus Development Conference Diagnosis 1993 Prohylaxis and treatment of osteoporosis. Am J Med **94:**646–650.
31. Mosekilde L, Mosekilde L, Danielsen CC 1987 Biomechanical competence of vertebral trabecular bone in relation to ash density and age in normal individuals. Bone **8:**79–85.
32. Wang XD, Masilamani NS, Mabrey JD, Alder ME, Agrawal CM 1998 Changes in the fracture toughness of bone may not be reflected in its mineral density, porosity and tensile properties. Bone **23:**67–72.
33. Goldstein SA 1987 The mechanical properties of trabecular bone formed at remodelling sites in normal human iliac trabecular bone: Variations with age and sex. J Biomech **20:**1055–1061.
34. Thomsen JS, Ebbesen EN, Mosekilde L 1998 Relationships between static histomorphometry and bone strength measurements in human iliac crest bone biopsies. Bone **22:**153–163.
35. Melton LJ, Kan SH, Frye MA, Wahner HW, O'Fallon WM, Riggs BL 1989 Epidemiology of vertebral fractures in women. Am J Epidemiol **129:**1000–1012.
36. Goulet RW, Goldstein SA, Ciarelli MJ, Kuhn JL, Brown MB, Feldkamp LA 1994 The relationship between the structural and orthogonal compressive properties of trabecular bone. LA J Biomech **27:**375–389.
37. Ulrich D, Van Rietbergen B, Laib A, Rüegsegger PA 1999 The ability of three-dimensional structural indices to reflect mechanical aspects of trabecular bone. Bone **25:**55–60.
38. Wachter NJ, Augat P, Mentzel M, Sarkar MR, Krischak GD, Kinzl L, Claes LE 2001 Predictive value of bone mineral density and morphology determined by peripheral quantitative computed tomography for cancellous bone strength of the proximal femur. Bone **28:**133–139.
39. Beck JD, Canfield BL, Haddock SM, Chen TJH, Kothari M, Keaveny TM 1997 Three-dimensional imaging of trabecular bone using the computer numerically controlled milling technique. Bone **21:**281–287.
40. Müller R, Hildebrand T, Rüegsegger P 1994 Non-invasive bone biopsy: a new method to analyze and display the three-dimensional structure of trabecular bone. Phys Med Biol **39:**145–164.
41. Lang T, Augat P, Majumdar S, Ouyang X, Genant HK 1998 Noninvasive assessment of bone density and structure using computed tomography and magnetic resonance. Bone **22:**149S–153S.
42. Majumdar S, Newitt DC, Jergas MD, Gies AA, Chiu E, Osman D, Keltner J, Keyak JH, Genant HK 1995 Evaluation of technical factors affecting the quantification of trabecular bone structure using magnetic resonance imaging. Bone **17:**417–430.
43. Parfitt AM, Mathews CHE, Villanueva AR, Kleerekoper M, Frame B, Rao DS 1983 Relationships between surface, volume, and thickness of iliac trabecular bone in aging and in osteoporosis. J Clin Invest **72:**1396–1409.
44. Kleerekoper M, Villanueva AR, Stanciu J, Rao DS, Parfitt AM 1985 The role of three-dimensional trabecular microstructure in pathogenesis of vertebral compression fractures. Calcif Tissue Int **37:**594–597.
45. DeHoff RT, Aigeltinger EH, Craig KR 1972 Experimental determination of the topological properties of three-dimensional microstructures. J Microsc **95:**69–91.
46. Feldkamp LA, Goldstein SA, Parfitt AM, Jesion G, Kleerekoper M 1994 The direct examination of three-dimensional bone architecture in vitro by computed tomography. J Bone Miner Res **4:**3–11.
47. Ito M, Nakamura T, Matsumoto T, Tsurusaki K, Hayashi K 1998 Analysis of trabecular microarchitecture of human iliac bone using microcomputed tomography in patients with hip arthrosis with or without vertebral fracture. Bone **23:**163–169.
48. Müller R, Van Campenhout H, Van Damme B, Van Der Perre G, Dequeker J, Hildebrand T, Ruegsegger P 1998 Morphometric analysis of human bone biopsies: A quantitative structural comparison of histological sections and micro-computed tomography. Bone **23:**59–66.
49. Hildebrand T, Laib A, Muller R, Dequeker J, Ruegsegger P 1999 Direct three-dimensional morphometric analysis of human cancellous bone: Microstructural data from spine, femur, iliac crest, and calcaneus. J Bone Miner Res **14:**1167–1174.
50. Bravenboer N, Papapoulos SE, Holzmann P, Hamdy NA, Netelenbos JC, Lips P 1999 Bone histomorphometric evalua-

tion of pamidronate treatment in clinically manifest osteoporosis. Osteoporos Int **9:**489–493.
51. Glimcher MJ 1998 The nature of the mineral phase in bone. In: Glimcher MJ (eds.) Metabolic Bone Disease. Academic Press, San Diego, CA, USA, pp. 23–50.
52. Lafage MH, Balena R, Battle MA, Shea M, Seedor JG, Klein H, Hayes WC, Rodan GA 1995 Comparison of alendronate and sodium fluoride effects on cancellous and cortical bone in minipigs. A one-year study. J Clin Invest **95:**2127–2133.
53. Rath NC, Balog JM, Huff WE, Huff GR, Kulkarni GB, Tierce JF 1999 Comparative differences in the composition and biomechanical properties of tibiae of seven- and seventy-two-week-old male and female broiler breeder chickens. Poult Sci **78:**1232–1239.
54. Wojtowicz A, Dziedzic-Goclawska A, Kaminski A, Stachowicz W, Wojtowicz K, Marks SC Jr, Yamauchi M 1997 Alteration of mineral crystallinity and collagen cross-linking of bones in osteopetrotic toothless (tl/tl) rats and their improvement after treatment with colony stimulating factor-1. Bone **20:**127–132.
55. Wassen MH, Lammens J, Tekoppele JM, Sakkers RJ, Liu Z, Verbout AJ, Bank RA 2000 Collagen structure regulates fibril mineralization in osteogenesis as revealed by cross-link patterns in calcifying callus. J Bone Miner Res **15:**1776–1785.

Address reprint requests to:
Françoise Peyrin, Ph.D.
ESRF, BP 220
38043 Grenoble Cedex, France